ACS OMEGA

http://pubs.acs.org/journal/acsodf

Article

Photocatalytic Deposition of Nanostructured $CsPbBr_3$ Perovskite Quantum Dot Films on Mesoporous TiO_2 and Their Enhanced Visible-Light Photodegradation Properties

Johan R. Gonzalez-Moya, Chen-Yu Chang, Daniela R. Radu, and Cheng-Yu Lai*

Cite This: *ACS Omega* 2022, 7, 26738−26748

Read Online

ACCESS | Metrics & More | Article Recommendations | Supporting Information

ABSTRACT: Herein, we report the in situ photocatalytic deposition of cesium lead bromide ($CsPbBr_3$) perovskite quantum dots on mesoporous TiO_2-coated fluorine-doped tin oxide (FTO/TiO_2) electrodes. The mesoporous TiO_2 layer is used as a photocatalyst to promote the following: (1) the Pb deposition from a Pb^{2+} aqueous solution and (2) the in situ Pb conversion into $CsPbBr_3$ perovskite in the presence of a CsBr methanolic solution without any organic capping agent. Both steps are carried out under ultraviolet light irradiation under ambient conditions without any post-treatment. The obtained FTO/TiO_2/$CsPbBr_3$ film was characterized by UV−vis diffuse reflectance spectroscopy, X-ray diffraction, photoluminescence spectroscopy, scanning electron microscopy, and transmission electron microscopy. The FTO/TiO_2/$CsPbBr_3$ heterojunction exhibited enhanced visible-light photodegradation activity demonstrated for the oxidation of curcumin organic dye as a model system. The novel and simple approach to fabricating a supported photocatalyst represents a scalable general method to use semiconductors as a platform to incorporate different perovskites, either all-inorganic or hybrid, for optoelectronic applications. The perovskite deposition method mediated by the UV light at room temperature could be further applied to flexible and wearable solar power electronics.

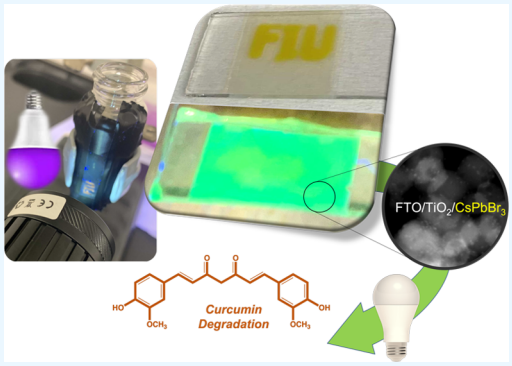

INTRODUCTION

Metal-halide perovskites have attracted great attention in the past two decades for many applications,[1−3] such as solar cells,[4−6] light-emitting diodes,[7,8] photodetectors,[9,10] and, most recently, photocatalysis,[11−13] due to their unique optoelectronic properties including tunable band gap, low exciton binding energy, and long carrier lifetime, along with simple preparation techniques and low material cost. All-inorganic halide perovskite quantum dots (QDs) have emerged in the past decade with promising stability if compared with their hybrid organic−inorganic perovskite counterparts.[14−16]

Titanium dioxide (TiO_2) is a semiconductor extensively used for the electron transport layer on perovskite solar cells due to the favorable band alignment for electron transfer and its good electron transport properties.[17,18] TiO_2 sensitized with halide perovskite QDs has been applied in visible-light-driven photocatalysis.[19−24] Schünemann et al. reported the use of a $CsPbBr_3$/TiO_2 composite for visible-light-driven photocatalytic benzyl alcohol oxidation.[19] Guo et al. investigated a $CsPbBr_3$/TiO_2 photocatalyst for visible-light photodegradation of rhodamine with better efficiency than a commercially available TiO_2 catalyst (P25) used as the reference material.[22] Also, the $CsPbBr_3$ QDs have been applied to photocatalytic degradation of tobacco tar alongside other semiconductors, like Bi_2WO_6.[25]

Both physical and chemical deposition methods were employed to sensitize TiO_2 electrodes with halide perovskite QDs films.[26,27] The chemical deposition methods, also known as solution-processing methods, are a more facile approach with greater possibilities for scale-up manufacturing. A typical deposition method is spin coating, where the halide perovskite bulk material precursors are dissolved in a polar solvent (often DMF, DMSO) followed by spin coating in a sequential way that allows in situ perovskite formation. The process involves an additional temperature annealing step to improve the perovskite crystallinity.[27] The spin coating methods are raising safety concerns because of the waste of the precursors containing Pb and toxic solvents.[28] Also, when spin coating is used for greater areas, the perovskite film thickness often is compromise.[29]

Electrodeposition methods for perovskites on TiO_2 electrodes have been proposed, especially for the preparation of the mixed halide perovskites.[30−34] Usually this method has two or more steps; in the first step, the Pb precursor is electro-

Received: May 17, 2022
Accepted: July 12, 2022
Published: July 21, 2022

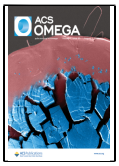

deposited as PbO_2[31] or metallic Pb[34] by oxidative or reductive electrodeposition technique, respectively. After the electrodeposition step, the lead-containing layer is chemically[31] or electrochemically[34] converted to lead halide and subsequently converted to the desired halide perovskite. Electrodeposition is a reproducible and relatively low-cost method, suitable for industrial large area coatings, and also avoids the waste of lead compounds because the deposited Pb is precisely controlled by the electrochemical parameters.

Aiming to reduce even more the perovskite processing costs and the development of greener processes, in this work, we have applied a photocatalytic deposition strategy to the direct fabrication of all-inorganic halide perovskites on a TiO_2 semiconductor scaffold for the first time. This simple and versatile method takes advantage of the photocatalytic properties of the TiO_2 and Pb redox behavior for depositing the metallic Pb precursor onto the mesoporous TiO_2 layer by photoreduction using only UV light without any electrochemical input. In the second step, the deposited Pb is converted to $CsPbBr_3$ perovskite by an in situ photocatalytic reaction mediated by TiO_2 photocatalysts and UV light. The $FTO/TiO_2/CsPbBr_3$ heterojunction obtained here presents enhanced visible-light photodegradation properties. This fast fabrication method has a great scalability potential and can be completely carried out in air at room temperature, using greener solvents and without any post-treatment. The proof-of-concept developed here may be applied to the photocatalytic deposition of perovskites for different optoelectronic applications and may use the solar energy not just for energy conversion in the solar cell but also for the perovskite sensitizer layer synthesis itself, reducing the overall cost to produce renewable energy.

MATERIALS AND METHODS

Materials. All chemicals used in the experiments were used as received, without further purification. Lead(II) acetate hexahydrate [$Pb(Ac)_2$, purity ≥ 98%], sodium acetate (NaAc), and cesium bromide (CsBr) were purchased from Alfa Aesar. Dimethylacetamide [DMAc, $CH_3CN(CH_3)_2$, ≥ 99.8%], dichloromethane (DCM, CH_2Cl_2 ≥ 99.0%), and hydroxypropyl cellulose, 80,000 MW, were ordered from Across Organics. Acetic acid, glacial (certified ACS), 2-propanol (C_3H_7OH, 99%), toluene, (C_7H_8, 99.5%), and methanol (CH_3OH, 99.8%) were bought from Fisher Scientific. Fluorine-doped tin oxide (FTO) glass with a sheet resistance of 15 Ω/sq was purchased from Hartford. Tetrabutylammonium hexafluorophosphate (NBu_4PF_6), for electrochemical analysis, ≥99.0% was bought from Millipore Sigma and the curcumin dye from TCI America. TiO_2 nanoparticles (15 nm) were purchased from US Research Nanomaterials, Inc.

Preparation of FTO/TiO_2 Electrodes. The mesoporous TiO_2-coated fluorine-doped tin oxide (FTO/TiO_2) electrodes were prepared using planar FTO with a sheet resistance of 15 Ω/sq. The mesoporous nanoTiO_2 films were fabricated on top of FTO as reported in the literature.[35] Briefly, TiO_2 nanoparticles (anatase, 15 nm diameter) were dispersed in a solution made of 5% hydroxypropyl cellulose (80,000 MW) in 2-propanol.

The dispersion was doctor-bladed onto the planar FTO substrate. After drying in air, the films were annealed at 400 °C for 3 h in ambient atmosphere.

Photocatalytic Deposition of $CsPbBr_3$ Perovskite QDs on FTO/TiO_2 electrodes. The $FTO/TiO_2/CsPbBr_3$ QDs films were obtained using a photocatalytic two-step method (Figure 1). In the first step, metallic Pb was deposited on the

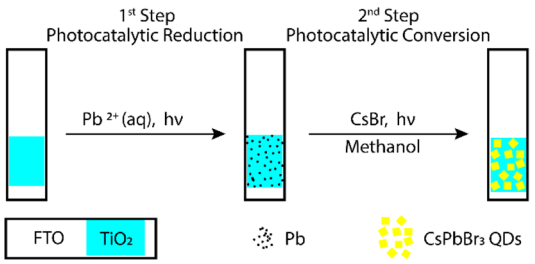

Figure 1. Schematic representation of the photocatalytic two-step method for $CsPbBr_3$ QDs deposition on FTO/TiO_2 electrodes. (See Supporting Information for SEM–EDX elemental mapping composition after both steps.)

mesoporous TiO_2 surface of the FTO/TiO_2 electrode by photocatalytic reduction of Pb^{2+} aqueous solution. In a typical experiment, the FTO/TiO_2 electrode was introduced into a clear vial containing 10 mM Pb^{2+} solution prepared in 0.1 M acetate buffer, with pH = 4.8. The electrode was then irradiated with a UV light (UVP EL Series, 4 W-302 nm) placed 1 cm away for 1, 3, 5, 10, 15, and 30 min in a series of different experiments. As a control experiment, an FTO/TiO_2 electrode was kept in the 10 mM Pb^{2+} solution for 30 min in the dark to compare with the samples obtained under UV light irradiation.

In the second step, an $FTO/TiO_2/Pb$ sample obtained using 1 min irradiation was converted into $CsPbBr_3$ QDs by an in situ photocatalytic conversion method. Briefly, a freshly prepared $FTO/TiO_2/Pb$ electrode was immersed in a 0.05 M CsBr methanol solution with 2% (v/v) of dimethylacetamide (DMAc) and irradiated with the same UV light source placed 1 cm away, for different times (1, 3, 5, 10, and 30 min). The DMAc was used to improve the crystallinity of the perovskite film.[36] The obtained $FTO/TiO_2/CsPbBr_3$ was rinsed with 2-propanol, dried in air, and stored in the dark for further material and photoelectrochemical (PEC) characterizations.

To prove that ultraviolet irradiation is required, in the second step, we designed two different control experiments. For the first, we kept the $FTO/TiO_2/Pb$ in the CsBr solution in the dark for 30 min to monitor the occurrence of any reaction. In the second control experiment, a photomask was used, enabling the UV light to pass only through the open window to the $FTO/TiO_2/Pb$ sample (FIU design) while blocking it in the masked area. This experiment aims to monitor any reaction occurring in the non-illuminated area of the sample.

Characterization. The crystal structure and purity of prepared $FTO/TiO_2/CsPbBr_3$ films were determined by X-ray powder diffraction (XRD) using a Rigaku MiniFlex diffractometer (Cu Kα radiation, λ = 1.5405 Å). The $FTO/TiO_2/CsPbBr_3$ film absorption was calculated using the Kubelka–Munk function from the diffuse reflectance spectra (DRS) obtained with a Shimadzu UV-3600 Plus UV–vis–NIR spectrophotometer. $BaSO_4$ was used as a reference standard for the DRS measurements. The photoluminescence (PL) characterization was carried out with an Edinburgh Instruments FS5 spectrofluorometer. The morphology and size of the synthesized $CsPbBr_3$ were determined by transmission electron microscopy (TEM) and high-resolution transmission

https://doi.org/10.1021/acsomega.2c03089
ACS Omega 2022, 7, 26738–26748

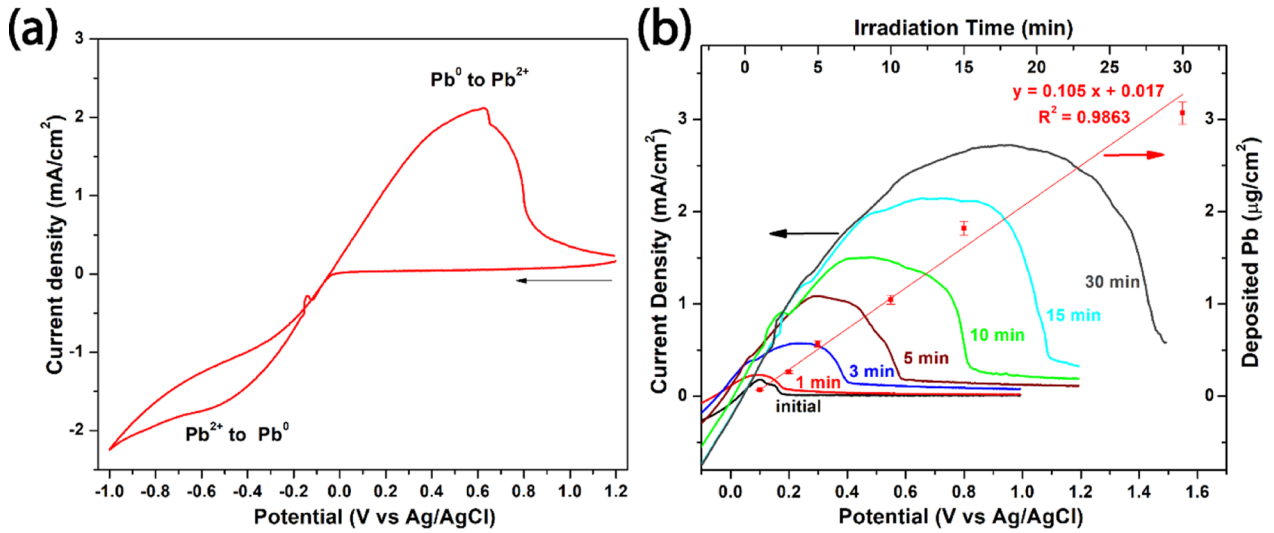

Figure 2. (a) CV from a Pb^{2+}/Pb redox couple on an FTO/TiO_2 electrode in 0.1 M acetate buffer (pH = 4.8). Scan rate: 20 mV/s. (b) LSV curves at 50 mV/s for the stripping of the photocatalytic deposited Pb after different UV irradiation times (scale bottom-left). Amount of Pb in $\mu g/cm^2$ deposited on the FTO/TiO_2 electrode after different UV irradiation times (scale up-right).

electron microscopy (HRTEM), using an FEI Talos F200X equipment; scanning electron microscopy (SEM) images were collected on a JEOL 6330F. Both the JEOL 6330F scanning electron microscope and FEI Talos F200X transmission electron microscope are equipped with energy dispersive spectroscopy (EDS), which enabled the determination of elemental distribution in the FTO/TiO_2/$CsPbBr_3$ samples.

Electrochemical experiments were performed with a Wave-Now Potentiostat (PINE research) using a three-electrode system in one compartment cell. The pristine FTO/TiO_2 or FTO/TiO_2/Pb samples were used as the working electrode, a graphite rod was used as a counter electrode, and Ag/AgCl (saturated KCl) was used as a reference electrode for the aqueous experiments.

For the photodegradation experiments, 3 mL of 10 ppm curcumin solution in toluene was placed in a quartz vial together with the photocatalyst FTO/TiO_2/$CsPbBr_3$ electrode and irradiated with visible light for 120 min. Before the visible-light irradiation, the sample was kept in the dark for 20 min to ensure that the adsorption−desorption equilibrium was reached. The visible-light source used was a white light lamp (UVP EL Series) with an intensity of 50 mW/cm^2 quantified using a Thor Labs silicon photodiode. At 20 min intervals, the UV−vis spectra of the solution were measured by UV−vis−NIR, using a Shimadzu UV3600 instrument to monitor the absorption maxima of curcumin at 417 nm. The ratio of curcumin concentration present in the solution at each time (C) to the initial concentration (C_0), that is, C/C_0, was determined from the ratio of the absorbance values measured in each interval and initial absorbance. PEC experiments were carried out using the same white light lamp as the visible-light source, placed at 1 cm of the working electrode. The working electrode was the pristine FTO/TiO_2 or FTO/TiO_2/$CsPbBr_3$ samples, a graphite rod was used as a counter electrode, and Ag wire was used as a pseudo-reference for the experiments. NBu_4PF_6 dissolved in DCM was used as the organic electrolyte.

RESULTS AND DISCUSSION

Photocatalytic Deposition of Pb on TiO_2 Electrodes. Cyclic voltammetry (CV) was used to initially investigate the electrochemical behavior of Pb^{2+} at FTO/TiO_2 electrodes. Figure 2a shows a CV for 10 mM $Pb(Ac)_2$ on FTO/TiO_2 electrode in 0.1 M acetate buffer, pH 4.8, as the electrolyte. The potential of the electrode was scanned negatively from 1.2 to −1.0 V versus Ag/AgCl and back again to the initial voltage at a scan rate of 20 mV/s. The forward scan of the CV showed a broad reduction shoulder around −0.5 V versus Ag/AgCl corresponding to the two-electron reduction of Pb^{2+} to metallic Pb(0).[37]

The reverse scan of CV also showed a very broad anodic peak current at approximately 0.6 V versus Ag/AgCl corresponding to the reoxidation of Pb(0) on the electrode surface back to the solution as Pb^{2+}.

It is well known that TiO_2 can be used as a photocatalyst for Pb^{2+} removal from the aqueous solution by reductive deposition of metallic Pb on the TiO_2 surface using light.[38−40] We took advantage of this property to deposit the metallic Pb on FTO/TiO_2 electrodes by only UV irradiation without applying any electrochemical potential, thus saving energy in the process. The photocatalytically deposited Pb serves as precursor to be subsequently converted to $CsPbBr_3$ perovskite QDs using also a photocatalytic method mediated by the mesoporous TiO_2 surface.

The amount of Pb deposited onto the FTO/TiO_2 electrode surface after UV irradiation at different times in a 10 mM Pb^{2+} acetate buffer solution was estimated by an electrochemical technique. Linear sweep voltammetry (LSV) from −0.1 to 1.2 V versus Ag/AgCl at 50 mV/s was acquired after each deposition time (Figure 2b). The oxidative sweep ensured the stripping of the photocatalytic deposited Pb onto the FTO/TiO_2 electrode back to the solution as Pb^{2+}. The charge (area under the peak) was determined from the LSV curves and plugged into Faraday's Law to obtain the amount of Pb in $\mu g/cm^2$ deposited on the FTO/TiO_2 electrode surface, according to the following equation

https://doi.org/10.1021/acsomega.2c03089
ACS Omega 2022, 7, 26738−26748

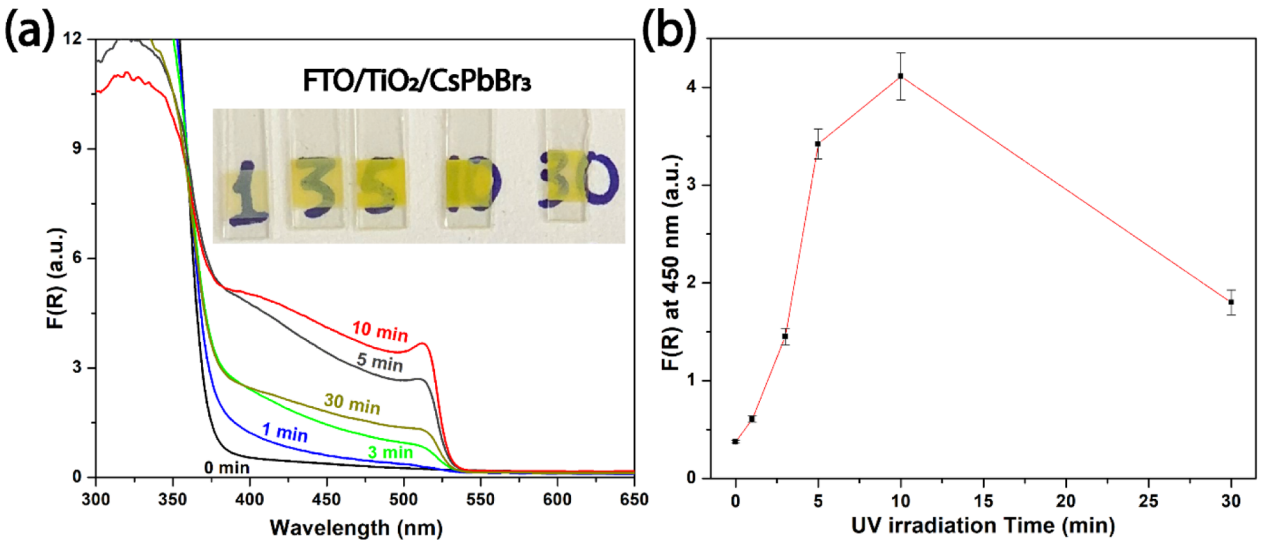

Figure 3. (a) DRS spectra of the samples with different UV irradiation times. (b) F(R) at 450 nm for the samples with different UV irradiation times.

$$m(\mathrm{Pb})_{\mathrm{deposited}} = \frac{Q \times M(\mathrm{Pb}) \times 10^6}{F \times z \times A} \quad (1)$$

where Q is a charge (area under the peak) in C, $M(\mathrm{Pb})$ = 207.2 g/mol is a Pb atomic mass, F = 96485 C/mol is Faraday's constant, z = 2 is the number electrons transferred per Pb atom in the oxidation step, and A = 1 cm^2 is a geometrical area of the FTO/TiO_2 electrode.

Figure 2b (scale up-right) depicts the amount of Pb in μg/cm^2 deposited on the FTO/TiO_2 electrode after different times of UV irradiation estimated by the LSV curves. The graph shows that with increasing UV irradiation from 1 to 30 min, the amount of deposited Pb increases almost linearly from 0.07 to 3.07 μg/cm^2 (Table S1), with a rate of 0.1 μg/cm^2 per minute for our experimental conditions. As a control experiment, we kept the FTO/TiO_2 in the 10 mM Pb^{2+} solution for 30 min in the dark, and no significant difference between the initial and final LSV was obtained. This observation means that no perceptible amount of Pb was deposited on the FTO/TiO_2 electrode in the dark corroborating that the UV light irradiation is indispensable for the Pb^{2+} reduction reaction.

To corroborate the presence of Pb in the FTO/TiO_2/Pb (obtained with 1 min of UV irradiation) sample, top-view SEM imaging with elemental mapping EDX was carried out (Figure S1). The EDX elemental mapping shows the presence of Pb homogeneously distributed on the FTO/TiO_2/Pb sample together with the Ti and O elements, proving that the photoreduction of the Pb^{2+} in the first step is successful and occurs onto the entire irradiated area.

Pb deposition occurs as a result of a light-assisted process, entailing first the UV light absorption by the TiO_2, which results in excited electrons and holes. Next, photogenerated electrons reduce the Pb^{2+} to Pb(0) and the photogenerated holes are further oxidizing H_2O (O_2 evolution). After 30 min of UV irradiation, bubbles were spotted on the surface of the FTO/TiO_2 electrode, suggesting that the O_2 evolution reaction happens together with the Pb deposition.

The experimental evidence leads us to propose the following mechanism for the photocatalytic deposition of Pb on the FTO/TiO_2 electrodes, agreeing with previous studies.[40]

$$TiO_2 + \text{light} \rightarrow TiO_2(h^+ + e^-) \quad (2)$$

$$Pb^{2+} + 2\,e^- \rightarrow Pb(s) \quad (3)$$

$$O_2 + e^- \rightarrow {}^{\cdot}O_2^- \quad (4)$$

$$H_2O + h^+ \rightarrow {}^{\cdot}OH + H^+ \quad (5)$$

$$H_2O + 2h^+ \rightarrow 1/2O_2(g) + 2H^+ \quad (6)$$

In Situ Photocatalytic Conversion of Pb into $CsPbBr_3$ Perovskite QDs on FTO/TiO_2 Electrodes. The second step of the reaction is the in situ photocatalytic conversion of Pb to $CsPbBr_3$ perovskite QDs. Samples of FTO/TiO_2/Pb obtained with 1 min of UV irradiation were selected for the study and optimization of the second step. The Pb deposition time was limited to 1 min to ensure that the Pb is fully consumed in the conversion to $CsPbBr_3$. Different FTO/TiO_2/Pb samples were subsequently in situ photocatalytic-converted to FTO/TiO_2/$CsPbBr_3$ by UV light irradiation in the presence of the CsBr precursor during different times (1, 3, 5, 10, and 30 min). The inset in Figure 2a shows a picture of the samples obtained with different UV irradiation times. The $CsPbBr_3$ sample obtained with 1 min of UV irradiation shows a light-yellow color, indicating the formation of the $CsPbBr_3$ QDs heterostructure perovskite. After increasing the UV irradiation time to 10 min, a more homogeneous and bright yellow color in the entire TiO_2 electrode area is observable for the samples obtained with 3, 5, and 10 min of UV irradiation time.

Finally, for the 30 min UV irradiation time, a slight degradation of the perovskite layer occurs, as observed in the inhomogeneous, partially degraded yellow color film. According to literature, $CsPbBr_3$ perovskite degradation could be ascribed to the longer exposure to methanol (polar solvent) together with the UV light irradiation for a longer time.[41,42]

The optical absorption of the samples was investigated by UV−Vis diffuse reflectance spectroscopy (DRS) (Figure 3a). The FTO/TiO_2/$CsPbBr_3$ samples show absorption in the visible region with an edge around 530 nm if compared with the pristine FTO/TiO_2 that absorbs only in the UV region with an absorption edge around 380 nm. Figure 3b shows the absorbance at 450 nm versus the UV irradiation time for the

https://doi.org/10.1021/acsomega.2c03089
ACS Omega 2022, 7, 26738−26748

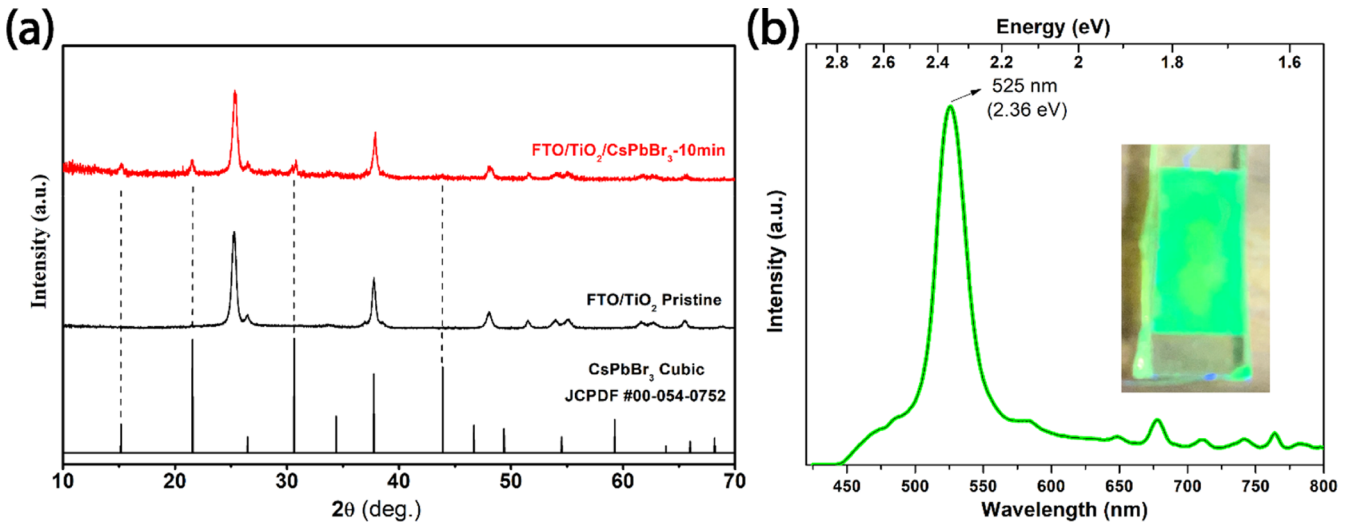

Figure 4. (a) XRD pattern of the samples. (b) PL spectra of the FTO/TiO_2/$CsPbBr_3$ sample at an excitation of 400 nm. Inset: image of the FTO/TiO_2/$CsPbBr_3$ sample under UV lamp excitation.

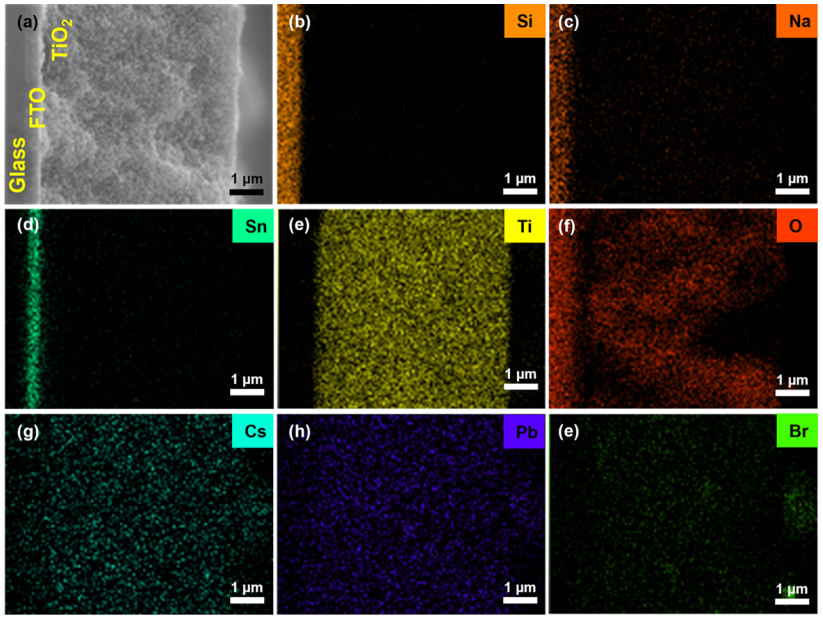

Figure 5. (a–i) Cross-sectional SEM image and EDX elemental mapping of Si, Na, Sn, Ti, O, Cs, Pb, and Br for the FTO/TiO_2/$CsPbBr_3$ sample.

different samples. It can be observed that the absorption of the samples increases until reaching 10 min of reaction, while for the 30 min of reaction time, the sample absorption is comparable with the 3 min sample. The quantitative analysis of the absorption confirms the qualitative trend that homogeneous $CsPbBr_3$ is obtained within 5 to 10 min of UV irradiation.

The band gap of the samples was calculated using a Tauc plot (Table S1).[43] For the pristine FTO/TiO_2 sample, a band gap of 3.21 eV (using an indirect semiconductor plot) was estimated, corresponding to the anatase TiO_2 layer.[44] In the case of the FTO/TiO_2/$CsPbBr_3$ samples, a band gap energy around 2.35 eV (using a direct semiconductor plot) was estimated, in agreement with literature-reported values for the $CsPbBr_3$ perovskite layer.[3]

The samples obtained with 10 min of UV irradiation time were chosen for further characterization of FTO/TiO_2/$CsPbBr_3$ (unless otherwise stated).

Figure 4a shows the XRD pattern of the pristine FTO/TiO_2 and the FTO/TiO_2/$CsPbBr_3$ samples. By comparison, it can be observed that after the in situ photocatalytic conversion, new peaks arise at 15.2, 21.6, 30.6, and 43.9° corresponding to the (100), (110), (200), and (220) crystal planes of cubic-phase $CsPbBr_3$ NCs (JCPDS no. 54-0752). An average of 22 nm for the coherent diffraction crystallite domain sizes was obtained using the Scherrer equation for the (110) crystal face of cubic $CsPbBr_3$.[45] The XRD results confirm the formation of $CsPbBr_3$ perovskite nanocrystals on top of the FTO/TiO_2 anatase electrode.

The PL spectrum (Figure 4b) of FTO/TiO_2/$CsPbBr_3$ sample shows a narrow emission at 525 nm with an FWHM of 25 nm at an excitation wavelength of 400 nm, agreeing with previous reports for $CsPbBr_3$ perovskite materials.[6] Accordingly, the FTO/TiO_2/$CsPbBr_3$ sample showed a bright green fluorescence under a manual UV light lamp irradiation (inset of Figure 4b).

https://doi.org/10.1021/acsomega.2c03089
ACS Omega 2022, 7, 26738−26748

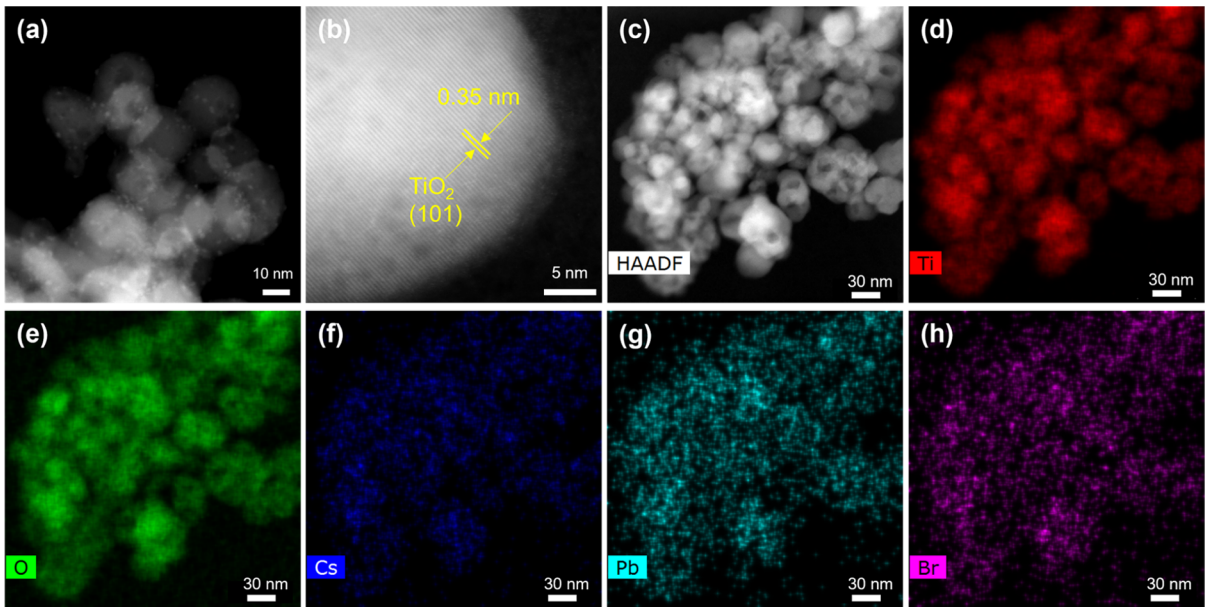

Figure 6. (a) TEM, (b) HRTEM, and (c–h) STEM–EDX elemental mapping images of Ti, O, Cs, Pb, and Br for the $TiO_2/CsPbBr_3$ heterostructure.

The ambient stability of the FTO/TiO_2/$CsPbBr_3$ sample without special storage conditions was monitored for 1 week by XRD and UV–vis absorption measurements (Figure S2). From the figure, we can observe that the XRD peaks of the cubic $CsPbBr_3$ phase are still present after 7 days but with less intensity. Also, the UV–vis absorption peak after 7 days is similar in shape to the initial sample with a little less intensity. These results show that the obtained FTO/TiO_2/$CsPbBr_3$ perovskite sample exhibits good ambient stability within a week after synthesis, thus suitable for applications under ambient conditions.

Figure S3 shows the top-view SEM images of the pristine FTO/TiO_2, FTO/TiO_2/Pb, and FTO/TiO_2/$CsPbBr_3$ samples, respectively. In all the images, we can see the nanoparticles of TiO_2 forming the mesoporous layer, but no significant difference is observed with the conversion of Pb to the $CsPbBr_3$ perovskite. This result is expected as the perovskite forms an ultra-thin, nanostructure layer on the TiO_2 surface. After the in situ photocatalytic conversion to the $CsPbBr_3$ perovskite, we can observe in the EDX elemental mapping (Figure S3d–i) the presence of the Cs, Pb, and Br elements homogeneously distributed together with the matrix of Ti and O elements, suggesting that the conversion to the $CsPbBr_3$ perovskite occurs in the second step of the reaction in the entire irradiated area where the Pb was previously deposited by photoreduction (in the first step of the process).

To investigate if the $CsPbBr_3$ perovskite deposition takes place only on the top surface of the electrode or within the entire mesoporous TiO_2 scaffold, cross-sectional SEM images together with EDX elemental mapping of the FTO/TiO_2/$CsPbBr_3$ sample were analyzed (Figure 5).

In the cross-sectional SEM image (Figure 5a), three well-defined layers could be observed, from left to right: a layer of the glass, which is the Supporting Information for the electrode, a 0.5 μm thick FTO layer, and the 5 μm thick mesoporous TiO_2 layer. The EDX elemental mapping also corroborates the three well-defined layers (Figure 5b–f), First, from the left, we can observe the presence of the Si and Na elements, matching the composition of silica glass. Next, we can observe the Sn element matching the region of the FTO layer and the Ti element perfectly the mesoporous TiO_2 layer. Lastly, we can observe the Cs, Pb, and Br elements from the $CsPbBr_3$ perovskite homogeneously distributed across the entire cross section of the mesoporous TiO_2 layer. The elemental composition of the $TiO_2/CsPbBr_3$ film, measured in the middle region of the cross section (2.5 μm), is shown in Table S3 (Supporting Information). This result proves that the $CsPbBr_3$ QDs impregnate all the mesoporous TiO_2 scaffolds and not only a few nanometers of the top surface, promoting a large surface area of the $TiO_2/CsPbBr_3$ heterojunction interface.

Figure 6a shows the TEM image of the $TiO_2/CsPbBr_3$ composite (sample scratched from the electrode) collected for studying the size and morphology of the $CsPbBr_3$ nanocrystals. The image shows the larger TiO_2 particles (around 20 nm) covered with very small (around 2 nm) $CsPbBr_3$ nanocrystals. Given that the sample preparation involved probe ultrasonication of the scraped sample in hexanes before deposition of the particles on the TEM grid, the process likely separated potentially larger particles (suggested by the XRD evaluation) at the surface of the $TiO_2/CsPbBr_3$ particles, keeping only the immediately attached small ones on the surface of the TiO_2.

HRTEM image of the $TiO_2/CsPbBr_3$ particles (Figure 6b) shows an interplanar distance of 0.35 nm corresponding to the (101) family of planes of anatase TiO_2.[46]

The planes for the cubic $CsPbBr_3$ perovskite were not identified in the HRTEM images due to the small size of the particles and also because the family of planes (111) with an interplanar distance of 0.34 nm (JCPDS no. 54-0752) is very similar to the (101) plane of anatase TiO_2. The similarity of the d spacing and the small size of the $CsPbBr_3$ NCs makes the proper identification very challenging.

Figure 6c–h shows the STEM–EDX elemental mapping images of Ti, O, Cs, Pb, and Br for the $TiO_2/CsPbBr_3$ heterostructure. We can observe that for the Ti and O elements, the corresponding colors are brighter and perfectly match the HAADF–STEM image, proving that the bigger particles correspond to the anatase TiO_2. Also, Cs, Pb, and Br

https://doi.org/10.1021/acsomega.2c03089
ACS Omega 2022, 7, 26738–26748

are present homogeneously throughout the sample, confirming that the impregnation of mesoporous TiO_2 with $CsPbBr_3$ QDs is successful over the entire surface area of the TiO_2 mesoporous layer.

The different characterization techniques discussed above show that a $CsPbBr_3$ perovskite QD film was obtained on FTO/TiO_2 substrates via the in situ photocatalytic conversion method. While a homogeneous distribution is observed, the film appears to be formed of discrete QDs. The second step is based on the use of the TiO_2 substrate as a photocatalyst to re-oxidize the deposited Pb in the first step back to Pb^{2+} under UV irradiation. Because the photocatalytic reaction occurs in the presence of CsBr, the Pb^{2+} rapidly reacts with Cs and Br and crystallizes in a $CsPbBr_3$ perovskite cubic phase. The change in color from the white FTO/TiO_2/Pb into a yellow FTO/TiO_2/$CsPbBr_3$ sample occurs in minutes. Importantly, the reaction method does not require post-processing (chemical treatment or thermal annealing) to stabilize the $CsPbBr_3$ perovskite layer, and the whole process is conducted under ambient conditions using mostly green solvents.

To prove that the UV irradiation is also needed, in the second step, we designed two different control experiments. In the first, we kept the FTO/TiO_2/Pb in the CsBr solution for 30 min in the dark, and no perceptible change in color was perceived.

This result suggests that without the UV light, no conversion to the $CsPbBr_3$ perovskite takes place. To corroborate the above results, we carried out a second control experiment using a photomask (FIU pattern) where the UV light passed only through the letters, thus only selectively reaching the FTO/TiO_2/Pb sample. After 5 min of UV irradiation using the photomask, we obtained a yellow FIU pattern (Figure 7) at the center of the sample due to the in situ photocatalytic conversion of the Pb to the $CsPbBr_3$ perovskite only in the irradiated parts of the FTO/TiO_2/Pb sample.

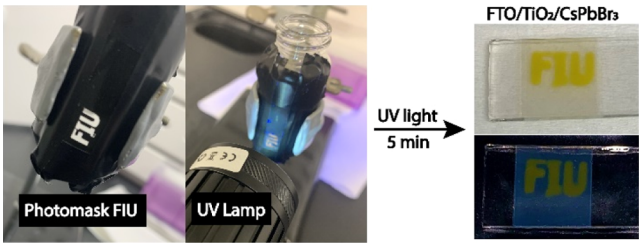

Figure 7. Control experiment uses a photomask (only the unmasked areas of the sample are exposed to UV irradiation through the FIU letter slit).

The results obtained from both control experiments prove that UV light irradiation is needed in order to convert the Pb into the $CsPbBr_3$ perovskite QDs. This is explained by an in situ photocatalytic mechanism mediated by the TiO_2 semiconductor. When the FTO/TiO_2/Pb sample is irradiated with UV light, some portion of the light will be absorbed by the TiO_2 photocatalyst and generate electrons and holes.

The photogenerated holes are used to oxidize the deposited Pb back to Pb^{2+}, which rapidly reacts with the $Cs^+$and Br^- precursors to form the $CsPbBr_3$ perovskite nanocrystals.

The proposed mechanism (the oxidative part) for the second step of the in situ photocatalytic conversion of Pb in the $CsPbBr_3$ perovskite in the FTO/TiO_2 substrates is shown below (eqs7−9)

$$TiO_2/Pb + light \rightarrow TiO_2/Pb(h^+ + e^-) \quad (7)$$

$$TiO_2/Pb + 2\,h^+ \rightarrow TiO_2/Pb^{2+} \quad (8)$$

$$TiO_2/Pb^{2+} + Cs^+ + 3Br^- \rightarrow TiO_2/CsPbBr_3 \quad (9)$$

PEC Activity of FTO/TiO_2/$CsPbBr_3$ Heterojunction. The FTO/TiO_2/$CsPbBr_3$ samples were further photoelectrochemically characterized to study the potential application of the heterojunction as a visible-light photocatalyst. Figure 8a shows the current−voltage ($I-V$) curves of the pristine FTO/TiO_2, FTO/TiO_2/Pb, and FTO/TiO_2/$CsPbBr_3$ samples. The LSV experiments were carried out in the 0.1 M NBu_4PF_6/DCM electrolyte solution at 20 mV/s, in the dark and under white light irradiation.

The results show that for the pristine FTO/TiO_2 sample, both $I-V$ curves are very similar with a small capacitive current for both experimental conditions. The $I-V$ curve shows that the FTO/TiO_2 sample does not develop any photocurrent under white light irradiation, making the sample inactive for visible-light photocatalysis. The above result was expected because the anatase TiO_2 (band gap 3.21 eV) absorbs light only in the ultraviolet region. For the FTO/TiO_2/Pb sample, we can observe for both experimental conditions a fast increase in the current around 0.75 V versus Ag/AgCl related to the Pb oxidation peak. The oxidation current is expected due to the Pb present in the sample after the photocatalytic reduction of the Pb^{2+} carried out in the first step of the reaction. This sample also does not show visible-light photocatalytic properties. On the other hand, for the FTO/TiO_2/$CsPbBr_3$ sample, the characteristic diode curve for photoactive semiconductor materials under visible-light irradiation can be observed.[11] In the $I-V$ curve, the photocurrent arises above the dark current level starting at −0.21 V and reaching a plateau (~40 $\mu A/cm^2$) in the 0.2−0.9 V potential region. After 0.9 V we can see an increase in the current that matches with the $I-V$ curve taken in the dark and also in the same region for the FTO/TiO_2/Pb sample. The increasing current at 0.9 V is related to the remnant Pb oxidation (Pb in excess, which does not react with the CsBr precursor and is not converted to the $CsPbBr_3$ perovskite).

The obtained characteristic diode curve (−0.2 to 0.9 V) proves that the FTO/TiO_2/$CsPbBr_3$ heterojunction is photoactive under visible-light irradiation, enhancing the performance of the pristine FTO/TiO_2 sample. This behavior is owed to the yellow $CsPbBr_3$ perovskite layer, absorbing visible light and generating electron/hole pairs, which are efficiently separated through the applied potential and instantly measured as a generated photocurrent.

Figure 8b shows the $I-V$ curve for the FTO/TiO_2/$CsPbBr_3$ sample under an on−off regime of white light irradiation. From the figure, we can observe that when the light is on, the current density increases almost instantly and drops again almost instantly to the dark current level when the light is off. This result confirms that the current is related to the visible-light stimuli and that the photo-response of the FTO/TiO_2/$CsPbBr_3$ electrode is very efficient.

The above PEC characterizations corroborate that the TiO_2 and $CsPbBr_3$ semiconductors form a heterojunction with an efficient interface for the electron transfer from the $CsPbBr_3$ nanocrystals to the mesoporous TiO_2 layer and thereafter to the FTO current collector, closing the circuit with the graphite counter electrode. The enhanced PEC properties of the FTO/

https://doi.org/10.1021/acsomega.2c03089
ACS Omega 2022, 7, 26738−26748

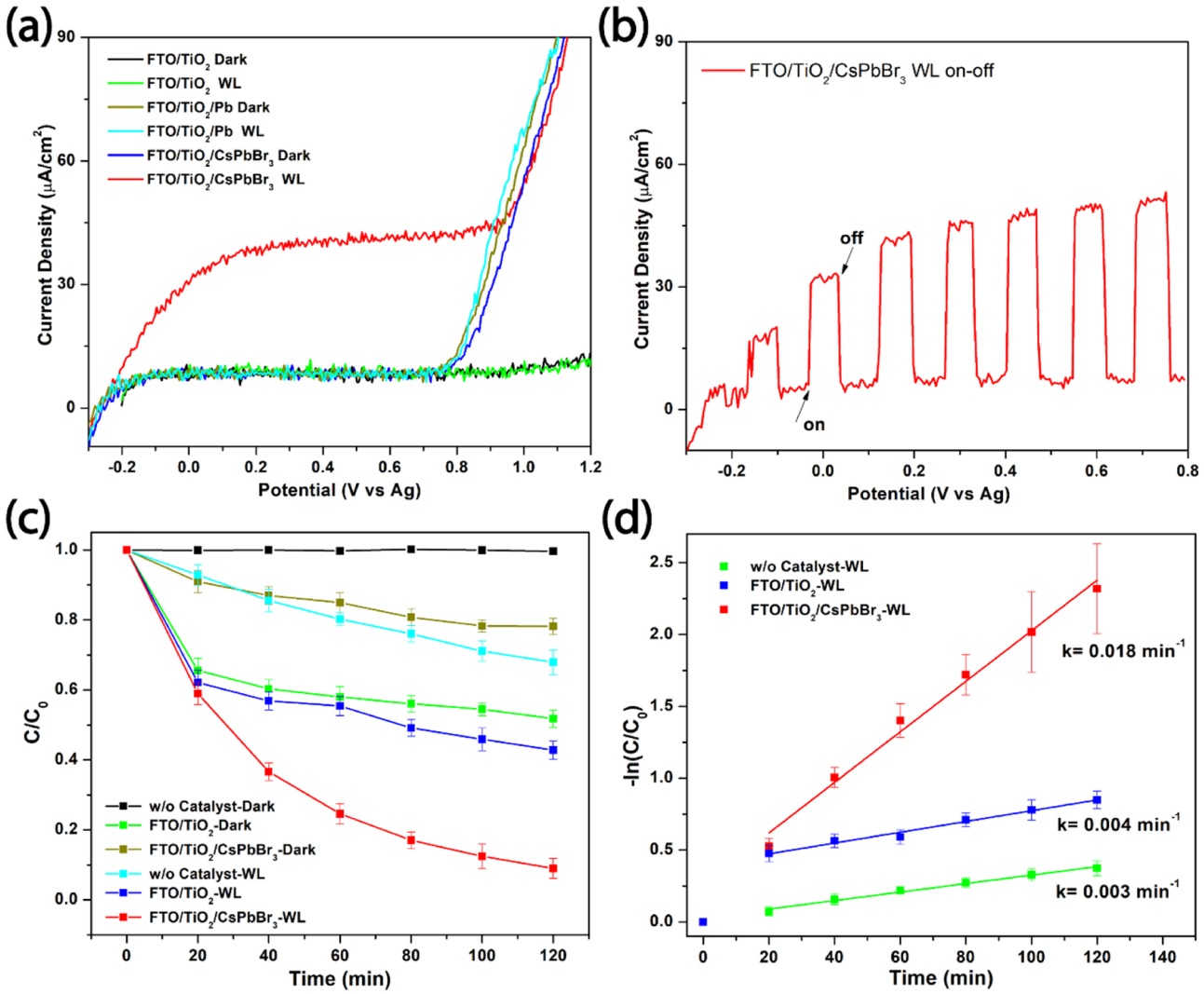

Figure 8. (a) Current−potential (I−V) curves for the different samples in dark and under white light irradiation. (b) Current−potential (I−V) curve under on−off cycles of white light irradiation for the FTO/TiO $_2$/$CsPbBr_3$ sample. (c) Photodegradation curves of curcumin by the different samples and experimental conditions. (d) Pseudo-first-order rate kinetics for the curcumin photodegradation with the different samples.

TiO_2/$CsPbBr_3$ sample toward a visible-light excitation make the heterojunction interesting for photocatalytic and solar cell applications.

Photodegradation Activity of FTO/TiO_2/$CsPbBr_3$ Samples. To study the organic photodegradation activity of the FTO/TiO_2/$CsPbBr_3$ sample with visible-light irradiation, curcumin, a natural dye, dissolved in toluene (yellow solution) was chosen as a model molecule. The curcumin dye has strong absorption in the visible domain of the spectrum with a maximum peak (λ_{max}) around 417 nm.[47] In a typical photodegradation experiment, the reduction of the maximum absorption peak was monitored as an indication of the degradation (decolorization) of the curcumin molecule in the toluene solution.

The ratio of the concentration of total curcumin present in the solution at any time (C) to the initial concentration (C_0), that is, C/C_0, was determined from the ratio of the absorbance values measured at 417 nm at different times during 120 min. The adsorption (dark condition) and photodegradation (white light irradiation) results obtained for the different experimental conditions are shown in Figure 8c.

By comparing the samples under dark conditions, we can observe that the pristine FTO/TiO_2 sample presents a greater adsorption capacity (48.2%) than the FTO/TiO_2/$CsPbBr_3$ sample (21.8%) due to the higher affinity of the curcumin to form bidentate (O−Ti−O) bonds with the titanium sites on the TiO_2 surface.[48] In the case of the FTO/TiO_2/$CsPbBr_3$ sample, the lower adsorption capacity is because of fewer Ti sites available on the TiO_2 surface now covered by the $CsPbBr_3$ perovskite nanocrystals. On the other hand, when we look at the curves under visible-light irradiation, first in the absence of any photocatalyst, the curcumin photodegradation is about 32.1%. The degradation of the curcumin by visible light is expected and reported for different solvents elsewhere.[47] Second, when the pristine FTO/TiO_2 was used as a photocatalyst, the photodegradation of the curcumin was 57.2%, only 1.2 times greater than the adsorption result from the dark experiment. This result suggests that the FTO/TiO_2 is not efficient as a visible-light-driven photocatalyst in agreement with the PEC results. Finally, when the FTO/TiO_2/$CsPbBr_3$ perovskite sample was used as a photocatalyst, the photodegradation of the curcumin was 91%. This value is 4.2 times greater than the value measured in the dark and 2.8 times

https://doi.org/10.1021/acsomega.2c03089
ACS Omega 2022, 7, 26738−26748

greater than the photodegradation of the organic curcumin with only the visible-light irradiation. The above results prove that the FTO/TiO_2/$CsPbBr_3$ sample is efficient as a visible-light-driven photocatalyst for the photodegradation of curcumin in toluene solvent.

Figure 8d shows the photodegradation curves under visible-light irradiation adjusted to the pseudo-first-order kinetic model. The kinetic constants extracted from the slope of the linear curves are shown in the graph (0.003, 0.004, and 0.018 min^{-1} for the self-degradation, pristine FTO/TiO_2, and FTO/TiO_2/$CsPbBr_3$ samples, respectively). The curcumin photodegradation rate using the FTO/TiO_2/$CsPbBr_3$ perovskite sample is 6 times higher than the self-degradation of the curcumin and 4.5 times higher than for the pristine FTO/TiO_2 sample, validating the performance of the FTO/TiO_2/$CsPbBr_3$ heterojunction sample as an efficient photocatalyst for organic degradation under visible-light irradiation as showed before through the PEC characterization. We posit that the mechanism for the visible-light-driven photodegradation of curcumin using the TiO_2/$CsPbBr_3$ heterostructure as a photocatalyst is aligned with previous literature findings. A schematic of the proposed mechanism is shown in Figure S4 (Supporting Information).[11,19,49]

The results described in this work proved the successful deposition of the $CsPbBr_3$ all-inorganic perovskite QD films onto FTO/TiO_2 substrates, using a novel in situ photocatalytic method, without the use of any post-treatment. The two-step method uses the mesoporous TiO_2 layer as a photocatalyst to enable Pb precursor deposition under ultraviolet irradiation in the first step. Subsequently, in the second step, the deposited Pb is converted to $CsPbBr_3$ under UV light irradiation in the presence of the CsBr methanolic solution by an in situ photocatalytic reaction mediated by the TiO_2 photocatalyst. The obtained FTO/TiO_2/$CsPbBr_3$ heterojunction shows enhanced properties toward organic molecule photodegradation and photocurrent generation under visible-light irradiation.

CONCLUSIONS

The present work provides a new, simple, and scalable strategy to deposit $CsPbBr_3$ all-inorganic perovskite QDs onto mesoporous TiO_2 films, using an in situ photocatalytic deposition method. In summary, the two-step photocatalytic method uses TiO_2 as a platform to photo-reduce the aqueous Pb^{2+} to metallic Pb and subsequently convert Pb to the $CsPbBr_3$ perovskite QDs film using UV light irradiation in both steps. The overall process takes place under ambient conditions and room temperature without the use of any post-treatment and any major toxic solvent, making the process a greener alternative to other perovskite deposition methods.

The FTO/TiO_2/$CsPbBr_3$ sample has successfully been applied as a visible photocatalyst for organic curcumin photodegradation, showing enhanced efficiency if compared with the pristine FTO/TiO_2. The FTO/TiO_2/$CsPbBr_3$ heterojunction also produces a higher photocurrent density than the pristine FTO/TiO_2 under visible-light irradiation, due to the improved electron excitation in the visible region, charge carrier separation, and transport efficiency. The concepts developed here can be extended to the photocatalytic deposition of different types of perovskite nanocrystals on top of different semiconductors on both rigid and flexible substrates, opening avenues for a myriad of applications in optoelectronics and solar photovoltaics.

ASSOCIATED CONTENT

Supporting Information

The Supporting Information is available free of charge at https://pubs.acs.org/doi/10.1021/acsomega.2c03089.

Top-view SEM images and EDX elemental mapping of the samples; deposited Pb and experimental E_g value tables; XRD pattern and DRS spectra of FTO/TiO_2/$CsPbBr_3$ sample at different times after being synthesized for stability test; elemental composition by EDX of the TiO_2/$CsPbBr_3$ sample; and proposed mechanism for the visible-light photodegradation of curcumin with TiO_2/$CsPbBr_3$ sample (PDF)

AUTHOR INFORMATION

Corresponding Author

Cheng-Yu Lai − *Department of Mechanical and Materials Engineering, Florida International University, Miami, Florida 33174, United States;* orcid.org/0000-0002-8931-5601; Email: clai@fiu.edu

Authors

Johan R. Gonzalez-Moya − *Department of Mechanical and Materials Engineering, Florida International University, Miami, Florida 33174, United States;* orcid.org/0000-0001-6387-1610

Chen-Yu Chang − *Department of Mechanical and Materials Engineering, Florida International University, Miami, Florida 33174, United States;* orcid.org/0000-0001-5253-1813

Daniela R. Radu − *Department of Mechanical and Materials Engineering, Florida International University, Miami, Florida 33174, United States;* orcid.org/0000-0001-6833-5825

Complete contact information is available at: https://pubs.acs.org/10.1021/acsomega.2c03089

Funding

The authors acknowledge funding from the National Science Foundation, Awards NSF CBET-1924412 and DMR-2122078, NASA Award #80NSSC19M0201, and NASA Award #80NSSC21M0310.

Notes

The authors declare no competing financial interest.

ACKNOWLEDGMENTS

The authors thank NSF and NASA for the funding, Prof. Christopher Dares at Florida International University for providing access to the white light source, Roberto Prado-Rivera at Florida International University for valuable discussions, and Dr. Ke Wang at the Pennsylvania State University for assisting with TEM images.

REFERENCES

(1) Vidyasagar, C. C.; Muñoz Flores, B. M.; Jiménez Pérez, V. M. Recent Advances in Synthesis and Properties of Hybrid Halide Perovskites for Photovoltaics. *Nano-Micro Lett.* **2018**, *10*, 68.

(2) Wang, X.; Zhang, T.; Lou, Y.; Zhao, Y. All-inorganic lead-free perovskites for optoelectronic applications. *Mater. Chem. Front.* **2019**, *3*, 365−375.

(3) He, X.; Qiu, Y.; Yang, S. Fully-Inorganic Trihalide Perovskite Nanocrystals: A New Research Frontier of Optoelectronic Materials. *Adv. Mater.* **2017**, *29*, 1700775.

(4) Yoo, S.-M.; Lee, S.-Y.; Kim, G.; Hernandez, E. V.; Mora-Seró, I.; Yoon, S. J.; Shin, T.; Lee, S.-H.; Ahn, S.; Song, M.-K.; et al. Preparation of nanoscale inorganic CsPbIxBr3-x perovskite photosensitizers on the surface of mesoporous TiO2 film for solid-state sensitized solar cells. *Appl. Surf. Sci.* **2021**, *551*, 149387.
(5) Aftab, A.; Ahmad, M. I. A review of stability and progress in tin halide perovskite solar cell. *Sol. Energy* **2021**, *216*, 26−47.
(6) Kumar, N.; Rani, J.; Kurchania, R. Advancement in CsPbBr3 inorganic perovskite solar cells: Fabrication, efficiency and stability. *Sol. Energy* **2021**, *221*, 197−205.
(7) Liu, X. K.; Xu, W.; Bai, S.; Jin, Y.; Wang, J.; Friend, R. H.; Gao, F. Metal halide perovskites for light-emitting diodes. *Nat. Mater.* **2021**, *20*, 10−21.
(8) Ji, K.; Anaya, M.; Abfalterer, A.; Stranks, S. D. Halide Perovskite Light-Emitting Diode Technologies. *Adv. Opt. Mater.* **2021**, *9*, 202002128.
(9) Wang, H. P.; Li, S.; Liu, X.; Shi, Z.; Fang, X.; He, J. H. Low-Dimensional Metal Halide Perovskite Photodetectors. *Adv. Mater.* **2021**, *33*, No. e2003309.
(10) Dong, Y.; Zou, Y.; Song, J.; Song, X.; Zeng, H. Recent progress of metal halide perovskite photodetectors. *J. Mater. Chem. C* **2017**, *5*, 11369−11394.
(11) Cardenas-Morcoso, D.; Gualdrón-Reyes, A. F.; Ferreira Vitoreti, A. B.; García-Tecedor, M.; Yoon, S. J.; Solis de la Fuente, M.; Mora-Seró, I.; Gimenez, S. Photocatalytic and Photoelectrochemical Degradation of Organic Compounds with All-Inorganic Metal Halide Perovskite Quantum Dots. *J. Phys. Chem. Lett.* **2019**, *10*, 630−636.
(12) Xu, F.; Meng, K.; Cheng, B.; Wang, S.; Xu, J.; Yu, J. Unique S-scheme heterojunctions in self-assembled TiO2/CsPbBr3 hybrids for CO2 photoreduction. *Nat. Commun.* **2020**, *11*, 4613.
(13) Zhang, Z.; Jiang, Y.; Shu, M.; Li, L.; Dong, Z.; Xu, J. Artificial Photosynthesis over Metal Halide Perovskites: Achievements, Challenges, and Prospects. *J. Phys. Chem. Lett.* **2021**, *12*, 5864−5870.
(14) Song, J.; Li, J.; Li, X.; Xu, L.; Dong, Y.; Zeng, H. Quantum Dot Light-Emitting Diodes Based on Inorganic Perovskite Cesium Lead Halides (CsPbX3). *Adv. Mater.* **2015**, *27*, 7162−7167.
(15) Protesescu, L.; Yakunin, S.; Bodnarchuk, M. I.; Krieg, F.; Caputo, R.; Hendon, C. H.; Yang, R. X.; Walsh, A.; Kovalenko, M. V. Nanocrystals of Cesium Lead Halide Perovskites (CsPbX(3), X = Cl, Br, and I): Novel Optoelectronic Materials Showing Bright Emission with Wide Color Gamut. *Nano Lett.* **2015**, *15*, 3692−3696.
(16) Lv, W.; Li, L.; Xu, M.; Hong, J.; Tang, X.; Xu, L.; Wu, Y.; Zhu, R.; Chen, R.; Huang, W. Improving the Stability of Metal Halide Perovskite Quantum Dots by Encapsulation. *Adv. Mater.* **2019**, *31*, No. e1900682.
(17) Kim, T.; Lim, J.; Song, S. Recent Progress and Challenges of Electron Transport Layers in Organic−Inorganic Perovskite Solar Cells. *Energies* **2020**, *13*, 5572.
(18) Raj, A.; Kumar, M.; Kumar, A.; Laref, A.; Singh, K.; Sharma, S.; Anshul, A. Effect of doping engineering in TiO2 electron transport layer on photovoltaic performance of perovskite solar cells. *Mater. Lett.* **2022**, *313*, 131692.
(19) Schünemann, S.; van Gastel, M.; Tüysüz, H. A CsPbBr3 /TiO2 Composite for Visible-Light-Driven Photocatalytic Benzyl Alcohol Oxidation. *ChemSusChem* **2018**, *11*, 2057−2061.
(20) Huang, H.; Verhaeghe, D.; Weng, B.; Ghosh, B.; Zhang, H.; Hofkens, J.; Steele, J. A.; Roeffaers, M. B. Metal Halide Perovskite Based Heterojunction Photocatalysts. *Angew. Chem., Int. Ed. Engl.* **2022**, *61*, No. e202203261.
(21) Li, Z. J.; Hofman, E.; Li, J.; Davis, A. H.; Tung, C. H.; Wu, L. Z.; Zheng, W. Photoelectrochemically Active and Environmentally Stable CsPbBr3/TiO2 Core/Shell Nanocrystals. *Adv. Funct. Mater.* **2017**, *28*, 1704288.
(22) Guo, Z.-a.; Zhang, B.; Li, H.; Ming, H.; Bala, H.; Yao, S.; Zhang, J.; Fu, W.; Cao, J.; Sun, G.; et al. Visible light responsive CsPbBr3/TiO2 photocatalyst with long-term stability in aqueous solution. *Mater. Lett.* **2020**, *274*, 128041.
(23) Bresolin, B.-M.; Park, Y.; Bahnemann, D. Recent Progresses on Metal Halide Perovskite-Based Material as Potential Photocatalyst. *Catalysts* **2020**, *10*, 709.
(24) Corti, M.; Bonomi, S.; Chiara, R.; Romani, L.; Quadrelli, P.; Malavasi, L. Application of Metal Halide Perovskites as Photocatalysts in Organic Reactions. *Inorganics* **2021**, *9*, 56.
(25) Huang, R.; Zhang, M.; Zheng, Z.; Wang, K.; Liu, X.; Chen, Q.; Luo, D. Photocatalytic Degradation of Tobacco Tar Using CsPbBr3 Quantum Dots Modified Bi2WO6 Composite Photocatalyst. *Nanomaterials* **2021**, *11*, 2422.
(26) Chaudhary, B.; Kshetri, Y. K.; Kim, H. S.; Lee, S. W.; Kim, T. H. Current status on synthesis, properties and applications of CsPbX3(X = Cl, Br, I) perovskite quantum dots/nanocrystals. *Nanotechnology* **2021**, *32*, 502007.
(27) Dunlap-Shohl, W. A.; Zhou, Y.; Padture, N. P.; Mitzi, D. B. Synthetic Approaches for Halide Perovskite Thin Films. *Chem. Rev.* **2019**, *119*, 3193−3295.
(28) Jiang, Y.; Remeika, M.; Hu, Z.; Juarez-Perez, E. J.; Qiu, L.; Liu, Z.; Kim, T.; Ono, L. K.; Son, D. Y.; Hawash, Z.; et al. Negligible-Pb-Waste and Upscalable Perovskite Deposition Technology for High-Operational-Stability Perovskite Solar Modules. *Adv. Energy Mater.* **2019**, *9*, 1803047.
(29) Hamukwaya, S. L.; Hao, H.; Zhao, Z.; Dong, J.; Zhong, T.; Xing, J.; Hao, L.; Mashingaidze, M. M. A Review of Recent Developments in Preparation Methods for Large-Area Perovskite Solar Cells. *Coatings* **2022**, *12*, 252.
(30) Chen, H.; Wei, Z.; Zheng, X.; Yang, S. A scalable electrodeposition route to the low-cost, versatile and controllable fabrication of perovskite solar cells. *Nano Energy* **2015**, *15*, 216−226.
(31) Lv, P.; Zhang, P.; Chen, Z.; Dong, S.; Liu, M.; Ma, J.; Cai, J.; Sun, F.; Li, S. The preparation of all-inorganic CsPbI2−xBr1+x perovskite solar cells based on electrodeposited PbO2 film. *Sol. Energy* **2020**, *207*, 618−625.
(32) Kosta, I.; Grande, H.; Tena-Zaera, R. Dimethylformamide-free processing of halide perovskite solar cells from electrodeposited PbI2 precursor films. *Electrochim. Acta* **2017**, *246*, 1193−1199.
(33) Charles, U. A.; Ibrahim, M. A.; Teridi, M. A. M. Electrodeposition of organic−inorganic tri-halide perovskites solar cell. *J. Power Sources* **2018**, *378*, 717−731.
(34) Wang, X.; Abbasi, S.; Zhang, D.; Wang, J.; Wang, Y.; Cheng, Z.; Liu, H.; Shen, W. Electrochemical Deposition of CsPbBr3 Perovskite for Photovoltaic Devices with Robust Ambient Stability. *ACS Appl. Mater. Interfaces* **2020**, *12*, 50455−50463.
(35) Farnum, B. H.; Wee, K. R.; Meyer, T. J. Self-assembled molecular p/n junctions for applications in dye-sensitized solar energy conversion. *Nat. Chem.* **2016**, *8*, 845−852.
(36) Liu, R.; Xu, K. Solvent engineering for perovskite solar cells: a review. *Micro Nano Lett.* **2020**, *15*, 349−353.
(37) Sivan, S. K.; Shankar, S. S.; N, S.; Kandambath Padinjareveetil, A.; Pilankatta, R.; Kumar, V. B. S.; Mathew, B.; George, B.; Makvandi, P.; Černík, M.; et al. Fabrication of a Greener TiO2@Gum Arabic-Carbon Paste Electrode for the Electrochemical Detection of Pb(2+) Ions in Plastic Toys. *ACS Omega* **2020**, *5*, 25390−25399.
(38) Murruni, L.; Conde, F.; Leyva, G.; Litter, M. I. Photocatalytic reduction of Pb(II) over TiO2: New insights on the effect of different electron donors. *Appl. Catal., B* **2008**, *84*, 563−569.
(39) Sreekantan, S.; Lai, C. W.; Mohd Zaki, S. The Influence of Lead Concentration on Photocatalytic Reduction of Pb(II) Ions Assisted by Cu-TiO2Nanotubes. *Int. J. Photoenergy* **2014**, *2014*, 839106.
(40) Zhang, H.; Wang, X.; Li, N.; Xia, J.; Meng, Q.; Ding, J.; Lu, J. Synthesis and characterization of TiO2/graphene oxide nanocomposites for photoreduction of heavy metal ions in reverse osmosis concentrate. *RSC Adv.* **2018**, *8*, 34241−34251.
(41) Sun, Y.; Zhang, H.; Zhu, K.; Ye, W.; She, L.; Gao, X.; Ji, W.; Zeng, Q. Research on the influence of polar solvents on CsPbBr3 perovskite QDs. *RSC Adv.* **2021**, *11*, 27333−27337.
(42) Esparza, D.; Sidhik, S.; López-Luke, T.; Rivas, J. M.; De la Rosa, E. Light-induced effects on crystal size and photo-stability of colloidal CsPbBr3 perovskite nanocrystals. *Mater. Res. Express* **2019**, *6*, 045041.

https://doi.org/10.1021/acsomega.2c03089
ACS Omega 2022, 7, 26738−26748

(43) Makula, P.; Pacia, M.; Macyk, W. How To Correctly Determine the Band Gap Energy of Modified Semiconductor Photocatalysts Based on UV-Vis Spectra. *J. Phys. Chem. Lett.* **2018**, *9*, 6814−6817.
(44) Parrino, F.; Pomilla, F. R.; Camera-Roda, G.; Loddo, V.; Palmisano, L. Properties of titanium dioxide. *Titanium Dioxide (Tio_2) and Its Applications*; Elsevier, 2021; pp 13−66.
(45) Nedelcu, G.; Protesescu, L.; Yakunin, S.; Bodnarchuk, M. I.; Grotevent, M. J.; Kovalenko, M. V. Fast Anion-Exchange in Highly Luminescent Nanocrystals of Cesium Lead Halide Perovskites (CsPbX3, X = Cl, Br, I). *Nano Lett.* **2015**, *15*, 5635−5640.
(46) Freitas, D. V.; González-Moya, J. R.; Soares, T. A. S.; Silva, R. R.; Oliveira, D. M.; Mansur, H. S.; Machado, G.; Navarro, M. Enhanced Visible-Light Photoelectrochemical Conversion on TiO2 Nanotubes with Bi2S3 Quantum Dots Obtained by in Situ Electrochemical Method. *ACS Appl. Energy Mater.* **2018**, *1*, 3636−3645.
(47) Mondal, S.; Ghosh, S.; Moulik, S. P. Stability of curcumin in different solvent and solution media: UV-visible and steady-state fluorescence spectral study. *J. Photochem. Photobiol., B* **2016**, *158*, 212−218.
(48) Lim, J.; Bokare, A. D.; Choi, W. Visible light sensitization of TiO2 nanoparticles by a dietary pigment, curcumin, for environmental photochemical transformations. *RSC Adv.* **2017**, *7*, 32488−32495.
(49) Scheidt, R. A.; Kerns, E.; Kamat, P. V. Interfacial Charge Transfer between Excited CsPbBr3 Nanocrystals and TiO2: Charge Injection versus Photodegradation. *J. Phys. Chem. Lett.* **2018**, *9*, 5962−5969.

https://doi.org/10.1021/acsomega.2c03089
ACS Omega 2022, 7, 26738−26748